Chemistry–A European Journal
Research Article
doi.org/10.1002/chem.202303455
Chemistry Europe
European Chemical Societies Publishing
www.chemeurj.org

Cu(I) Complexes Comprising tetrahedral Mo_2E_2 or Mo_2PE units (E = P, As, Sb) as Chelating Ligands

Bijan Mondal[a] and Manfred Scheer*[a]

Dedicated to Professor Klaus Köhler on the occasion of his 65th birthday.

Novel isomorphous tetranuclear complexes, [(dppf)Cu(μ_3,$\eta^{2:2:2}$-E_2{CpMo(CO)$_2$}$_2$]BF_4 [E = P (**1**), As (**4**), Sb (**5**), (dppf = 1,1′-bis-(diphenylphosphino)-ferrocene)] and [(dppf)Cu(μ_3,$\eta^{2:2:2}$-PE{CpMo(CO)$_2$}$_2$]BF_4 [E = As (**2**), Sb(**3**)] were synthesized from the reactions between [(dppf)Cu(MeCN)$_2$][BF_4] and tetrahedral molybdenum complexes containing unsubstituted homo- and hetero-diatomic group-15 elements [(μ,$\eta^{2:2}$-E_2{CpMo(CO)$_2$}$_2$] [E = P (**A**), As (**D**), Sb (**E**)] and [(μ,$\eta^{2:2}$-PE{CpMo(CO)$_2$}$_2$] [E = As (**B**), Sb (**C**)], respectively. In all these products, the {Mo_2E_2} or {Mo_2PE} moieties coordinate the Cu(I) center via a rare side-on η^2-coordination mode. The X-ray structure analyses of [(dppf)Cu-(μ_3,$\eta^{2:2:1}$-PSb{CpMo(CO)$_2$}$_2$][BF_4] demonstrate, for the first time, the utilization of an η^1-coordination mode for the ligand complex **C** to coordinate to the Cu(I) center. All the products were characterized by X-ray crystallography, NMR and IR spectroscopy, mass spectrometry and elemental analysis. Electrochemical studies also revealed the formation of **1**–**5**, and, further, to understand the structure and bonding of the products, theoretical calculations using density functional theory (DFT) were conducted.

Introduction

Substituent-free organometallic polyphosphorus (P_n) (n = 2–6) ligand complexes[1] showed their potential in the field of self-assembly[2] as useful connectors due to the localized electron pairs on each phosphorus atom.[3] In combination with coinage metal salts, the P_n-ligand complexes afforded 1D, 2D and 3D coordination polymeric networks[4] as well as organometallic-based nano-sized capsules and spherical cage molecules possessing inorganic fullerene-like cores.[5] The diverse chemistry was tuned depending on the coinage metal used, the nature and size of the anion as well as the stoichiometry and concentration of the reactions.[6] Among the P_n ligand complexes, the simplest diphosphorus complex, [$Cp_2Mo_2(CO)_4$(μ,$\eta^{2:2}$-P_2)] (Cp = η^5-C_5H_5), **A** was prepared by the thermolysis of [$Cp_2Mo_2(CO)_4$] in the presence of white P_4.[7] The coordination chemistry of **A** was extensively studied towards various coinage metal salts: CuX (X = Cl, Br, I), [Cu(MeCN)$_4$]X (X = TEF, BF_4, PF_6, TEF = [Al{OC(CF_3)$_3$}$_4$]), [Cu(MeCN)$_{3.5}$]FAL (FAL = FAl{$OC_6F_{10}(C_6F_5)$}$_3$), [Cu(o-DFB)]TEF (o-DFB = 1,2 difluorobenzene), AgX (X = TEF, FAL, CF_3SO_3, NO_3 PF_6, BF_4, ClO_4, SbF_6), Au(THT)Cl (THT = tetrahydrothiophene), [$(Ph_3P)_2$Au(THF)][PF_6], etc. that resulted in molecular, oligomeric or polymeric compounds.[8]

Recent results showed the ability of the tetrahedral hetero- and homo-dinuclear complexes [$Cp_2Mo_2(CO)_4$(μ,η^2:η^2-PE)][7,9] [E = P (**A**), As (**B**), Sb (**C**)] and [$Cp_2Mo_2(CO)_4$(μ,η^2:η^2-E_2)][10] [E = As (**D**) and Sb (**E**)] to bring two to four Cu(I)/Ag(I) centers in close proximity to achieve metallophilic[11] interactions demonstrating various modes of coordination.[12] The results showed that either the lone pairs located on the P or E atoms of the tetrahedral complexes or the P–E/E–E σ-orbital are donated to the coinage metal centers. Indeed, detailed theoretical calculations on **A**–**E** show that the lone pairs located on As and Sb atoms are lower in energy than that of the P atoms.[12b–c,e] Further, the inclusion of a heavier group 15 hetero-atom as in **B** and **C** elevated the energy of the P–E σ-bond. The higher σ(E–E) energy is, however, pronounced even in the heavier homo-diatomic congeners **D** and **E**. This indicates that σ(P–E)/ σ(E–E) bonds allow an effective orbital overlap with the unoccupied orbitals of Cu/Ag, rather than the lone pairs, which can be observed among the compounds shown in Chart 1.

The bidentate dppf ligand (dppf = 1,1′-bis-(diphenylphosphino)-ferrocene) is well known to provide chelate bite according to the geometric requirement of the metal.[13] Further, the phenyl moieties often provide useful stabilization through noncovalent π-π interactions. In addition, the central ferrocene part of the dppf ligand is useful for redox property studies.[14] The Cu(I) salt [(dppf)Cu(MeCN)$_2$][BF_4] represents an interesting binuclear complex where the tetrahedral Cu is connected to a chelating ligand, dppf and two labile MeCN ligands. Concerted or step-wise replacements of the labile acetonitrile ligands from [(dppf)Cu(MeCN)$_2$][BF_4] provide a way to insert up to two same or different tetrahedral complexes. Therefore, in this report, we explore the coordination ability of the tetrahedral complexes **A**–**E** towards [(dppf)Cu(MeCN)$_2$][BF_4] leading to the isomor-

[a] Dr. B. Mondal, Prof. Dr. M. Scheer
Institute of Inorganic Chemistry, University of Regensburg
93040 Regensburg (Germany)
E-mail: manfred.scheer@chemie.uni-regensburg.de
Homepage: http://www.uni-regensburg.de/chemie-pharmazie/anorganische-chemie-scheer

Supporting information for this article is available on the WWW under https://doi.org/10.1002/chem.202303455

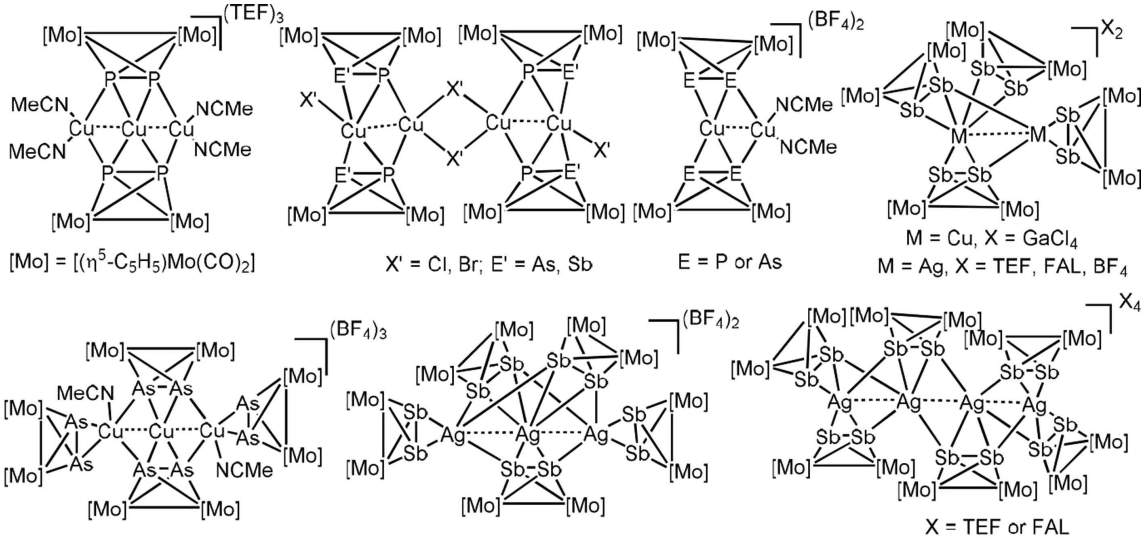

Chart 1. Unsubstituted homo- and hetero-diatomic molybdenum complexes supported metallophilic interactions.

phous tetranuclear compounds **1**–**5**. The results show that the central Cu(I) atom in **1**–**5** coordinates with a dppf ligand and an η^2-coordinated tetrahedral complex **A**–**E** depending on the choice of the tetrahedral complex. In addition, the molecular structure of **3** in the solid state shows an instance of an unprecedented η^1-coordination mode of **C**.

Results and Discussion

Although some of the tetrahedral molybdenum complexes **A**–**E** were known for a long time, not long since, our research group reported a general and effective route to prepare those complexes in good yields.[15] Therefore, depending on the availability of **A**–**E**, they were reacted with the Lewis-acidic Cu(I) salt $[(dppf)Cu(MeCN)_2][BF_4]$ to study the comparative reactivity of the tetrahedral molybdenum complexes. The reactions afforded the isostructural tetranuclear complexes **1**–**5** through the concerted replacement of the acetonitrile ligands by a tetrahedral molybdenum complex (Scheme 1). Syntheses, structural characterizations and electronic structures of **1**–**5** are discussed in the following.

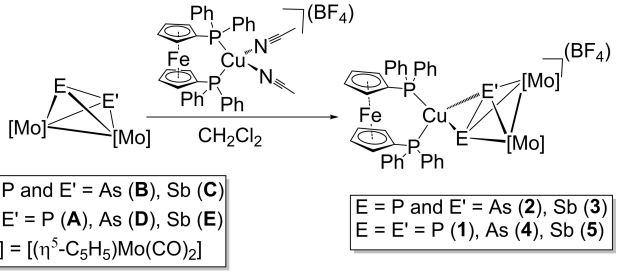

Scheme 1. Synthesis of **1**–**5**.

Syntheses and Characterizations of $[dppfCu(\mu_3,\eta^{2:2:2}\text{-}E_2\{CpMo(CO)_2\}_2]BF_4$ [E = P (1), As (4) and Sb (5)]

The orange-colored products **1**, **4**, and **5** are obtained in good to excellent yields (70–89%) when **A**, **D** and **E**, respectively, are reacted with $[(dppf)Cu(MeCN)_2][BF_4]$ in CH_2Cl_2. All the products were characterized by multinuclear NMR (^1H, ^{31}P, ^{13}C, ^{11}B and ^{19}F), IR, electrospray ionization mass spectrometry (ESI-MS), and single crystal X-ray crystallographic studies. The $^{31}P\{^1H\}$ NMR spectrum of compound **1** (Figure S8) at room temperature shows two singlets at −8.92 and −80.11 ppm which reveal the presence of dppf and **A** moieties, respectively. Note the distinct upfield shift of the signal for the P_2 unit in **1** as compared with $\delta = -43.7$ ppm (CD_2Cl_2) in the free **A**.[7] This indicates the coordination of the phosphorus atoms of **A** to the Cu(I) center. The ^1H NMR spectrum shows the signals due to phenyl groups ($\delta = 7.56$–7.45 ppm) as well as η^5-Cp ligands (Cp_2Fe: $\delta = 4.44$ and 4.26 ppm; {CpMo}: $\delta = 5.10$ ppm, Figure S7). The IR spectrum displays sharp bands in the carbonyl region (at 1966 and 1916 cm^{-1}, Figure S12), which further confirms the presence of the $\{CpMo(CO)_2\}$ moiety in **1**. The presence of the phenyl and Cp ligands was also confirmed by $^{13}C\{^1H\}$ NMR (Figure S9). The base peak in the ESI-MS+ at $m/z = 617.03$ is assigned to the $\{(dppf)Cu^+\}$ fragment. In addition, the mass spectrometry data shows the molecular ion peak at $m/z = 1116.85$ which is 499 units more than the base peak (Figure S13). This is attributed to the incorporation of one equivalent of **A** in **1** (molecular weight of **A** = 499.8), which is further confirmed by the calculated isotopic distribution pattern. The elemental analysis of **1** suggests a composition of $[(dppf)Cu(\mathbf{A})][BF_4]\bullet 2CH_2Cl_2$. The presence of the anion $[BF_4]^-$ is confirmed by $^{19}F\{^1H\}$ and $^{11}B\{^1H\}$ NMR spectroscopy as well as by negative mode ESI MS analysis (Figures S10 and S11). In order to confirm the spectroscopic assignments and to determine the solid-state structure of **1**, X-ray diffraction analysis was undertaken (Fig-

ure 1a) on the single crystals grown upon layering the crude reaction mixture (in CH_2Cl_2) with *n*-hexane.

Compound **1** crystallized in a monoclinic space group *C*2/*c* (Table 3). The solid-state structure shows a side-on η^2-*coordination* mode of the P_2 unit of **A** while binding to the {dppfCu} fragment. The central Cu atom adopts a pseudo-tetrahedral geometry which is reflected by the existence of different P–Cu–P bond angles [P04-Cu-P04′: 109.41(3), P05-Cu-P05′: 52.49(3), P05-Cu-P04: 101.13(2) and P05-Cu-P04: 147.50(2)°] and the Cu-P05 bond length of 2.4249(6) Å is found to be longer than the lengths observed in $[Cu_2\{(\mu,\eta^{2:2}\text{-}(\mathbf{A})\}_2\{\mu,\eta^2:\eta^1:\eta^1\text{-}(\mathbf{A})_2\}][TEF]$ (2.240(3)–2.277(2) Å). The observed P–P bond length of 2.1447(12) Å in **1** is slightly longer compared to one in the free ligand **A** (P–P in **A**: 2.079(2) Å),[7a] due to the side-on coordination. Such η^2-*coordination* mode of **A** could also be observed in $[Cu_2\{(\mu,\eta^{2:2}\text{-}(\mathbf{A})\}_2\{\mu,\eta^2:\eta^1:\eta^1\text{-}(\mathbf{A})_2\}][X]_2$ (X = PF_6, TEF, BF_4, FAL)[4f,6c,8a] where two η^2-coordinated **A** were found on both sides.

The coordination chemistry of the organometallic complexes containing 'naked' pnictogen atoms has been an area of intense research. However, studies on heavier congeners than P have only been sparingly explored due to the challenges involved related to their low yield and moderate air stability. Therefore, to enhance our knowledge, we targeted the reactivity of the mixed pnictogen ligand complexes **D** and **E** towards $[(dppf)Cu(MeCN)_2][BF_4]$ leading to the isolation of isomorphous compounds with the molecular formula $[dppfCu(\mu_3,\eta^{2:2:2}\text{-}(\mathbf{D})][BF_4]$ (**4**) (Figure 1b) and $[(dppf)Cu(\mu_3,\eta^{2:2:2}\text{-}(\mathbf{E})][BF_4]$ (**5**) (Figure 1c).

Compound **4** crystallizes in the monoclinic space group *C*2/*c* whereas compound **5** crystallizes in the orthorhombic space group *Pna*2$_1$. The E–E bonds in **D** (E = As) or **E** (E = Sb) are found to be simultaneously coordinated to a Cu atom in η^2-fashion. According to the CSD database,[16] η^2-coordination mode of **E** was also observed in four compounds, namely $[(\mathbf{E})(\mu\text{-CuX})]_2$ (X = Cl, Br), $[(\mathbf{E})(\mu\text{-CuI}_2)]_\infty$ and $[Cu_2(\eta^2\text{-}\mathbf{E})(\eta^{2:1}\text{-}\mathbf{E})_3][GaCl_4]_2$.[12a] Note that the only example of η^2-side-on coordinated **D** was observed in $[(MeCN)_2Cu_2\{(\mu,\eta^{2:2}\text{-}(\mathbf{D})\}_2)(Cu)\{\mu,\eta^2:\eta^2:\eta^1:\eta^1\text{-}(\mathbf{D})_2\}][BF_4]_3$,[12d] which is why **4** represents only the second example to date. Both the E–E bond distances found in **4** (As1-As1′ 2.3808(2) Å) and **5** (Sb1–Sb2: 2.75039(13) Å) are longer than that of free **D** and **E**, but comparable to the related compounds shown in Chart 1.

Although similar bite angles of the dppf ligand were observed (in **1**: 109.41(3), **4**: 110.281(18)° and **5**: (110.281(18)°), the E–Cu–E bond angle increases from **2** (P05-Cu-P05′ 52.49(3)°) to **4** (As1-Cu-As1 56.311(8)°) to **5** (Sb1-Cu1-Sb2 62.445(5)°). The Cu–As bond length of 2.5228(8) Å falls between 2.382(4) and 2.714(4) Å as observed in $[(MeCN)_2Cu_2\{(\mu,\eta^{2:2}\text{-}(\mathbf{D})\}_2)(Cu)\{\mu,\eta^2:\eta^2:\eta^1:\eta^1\text{-}(\mathbf{D})_2\}][BF_4]_3$. On the other hand, the observed Cu–Sb bond length of 2.6401(2) Å is slightly longer than that in $[(\mathbf{E})(\mu\text{-CuCl})]_2$ (2.6071(13)–2.889(13) Å). The ESI-MS + analyses of **4** and **5** show peaks at 1204.75 and 1296.71 (Figures S35 and S42) corresponding to the cationic part $[(dppf)Cu(\mathbf{D})]^+$ and $[(dppf)Cu(\mathbf{E})]^+$, respectively. The experimental isotopic distribution patterns of the fragments satisfactorily corroborated with the theoretical distribution.

Syntheses and Characterizations of $[dppfCu(\mu_3,\eta^{2:2:2}\text{-PE}\{CpMo(CO)_2\}_2]BF_4$ [E = As (2) and Sb (3)]

Replacing one of the P atoms in **A** by As or Sb showed an interesting coordination behavior of **B** and **C** in the presence of Lewis-acidic metal centers.[12b] It is structurally evident that both the lone pair electrons and the σ(P–E) bond can coordinate to more than one metal atom. This is in close agreement with the theoretical finding that the σ-bond energy of the P–E bond increases with the inclusion of the heavier group 15 elements and hence become potential donors.[12e] Therefore reactivities of **B** and **C** were performed towards $[(dppf)Cu(MeCN)_2][BF_4]$ affording compounds **2** and **3** in 79% and 80% yields, respectively (Scheme 1).

The identities of **2** and **3** were determined using single-crystal X-ray crystallographic analyses and confirmed by

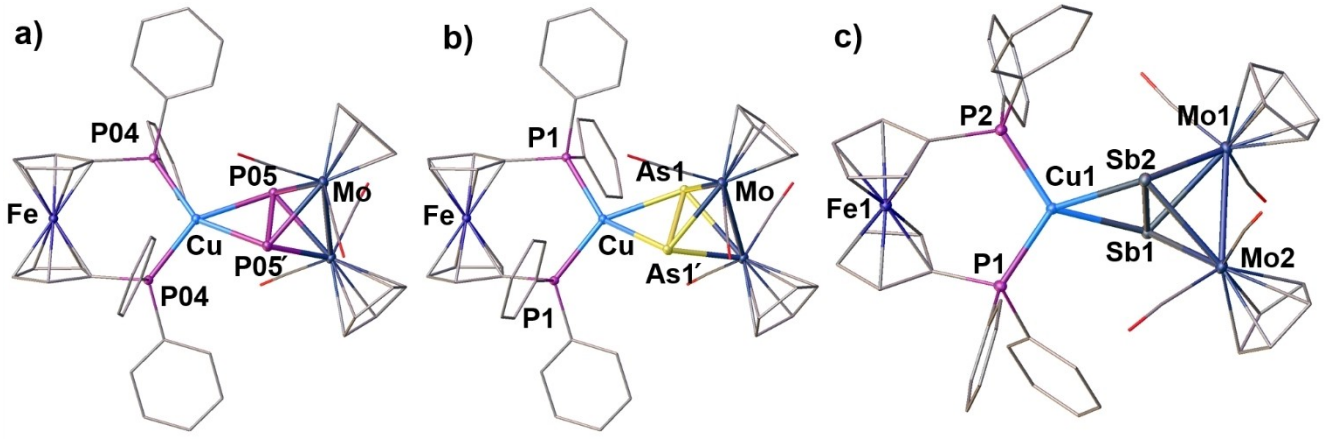

Figure 1. Solid-state structures of the cationic complexes (a) **1**, (b) **4** and (c) **5**. Ellipsoids are drawn at 50% probability (except for C and O atoms). Anion, BF_4 and the hydrogen atoms are omitted for clarity. Selected bond lengths (Å) and angles (°) of **1**: Mo-Mo 3.0347(4), Mo-P05 2.4665(6), Cu-P04 2.2912(6), Cu-P05 2.4251(7), P05-P05′2.1446(11), P04-Cu-P04′ 109.41(3), P04-Cu-P05 147.50(2), P05-Cu-P05′ 52.49(3); **4**: As1-As1′ 2.3808(2), Mo-Mo 3.0713(3), Mo-As1 2.63396(14), Cu-As1 2.5228(3), P1-Cu 2.2873(3), P1-Cu-P1′110.281(18), As1-Cu-As1′ 56.311(8), P1-Cu-As1 81.060(8); **5**: Sb1-Sb2 2.75039(13), Sb1-Mo1 2.84812(15), Sb1-Cu1 2.6401(2), Mo1-Mo2 3.11069(17), Cu1-P1 2.2743(4), P1-Cu1-Sb1 103.622(12), P2-Cu1-P1 113.014(17), Sb1-Cu1-Sb2 62.445(5).

elemental analysis, IR, NMR (^{1}H, ^{31}P, ^{13}C, ^{19}F and ^{11}B) and ESI-MS spectroscopy (Figures S14–S27). The IR spectra show sharp bands between 2048 and 1860 cm^{-1} corresponding to the stretching vibrations of the terminal CO ligands. The ^{1}H NMR spectrum displays the expected resonances characteristic of the cyclopentadienyl and phenyl groups. In the ^{31}P{^{1}H} NMR spectrum of **2**, the signal at $\delta = -22.63$ ppm (Figure S15) is assigned to the coordinated **B** which is found to be shifted in the upfield region compared to the free ligand. A similar trend in ^{31}P{^{1}H} NMR has also been observed for **3** (Table 1).

In the ESI-MS+ spectra of **2** and **3** in dichloromethane (Figures S20 and S27), the *m/z* values of 1160.798 and 1206.78 are attributed to the cationic fragments [dppfCu(**B**)]$^{+}$ and [dppfCu(**C**)]$^{+}$, respectively. Finally, the molecular structures of **2** and **3** were determined by single-crystal X-ray crystallography studies.

Table 1. Selected bond distances [Å] and ^{31}P{^{1}H} NMR [ppm] of **A**–**E** and **1**–**5**.

Compounds	P–E/E–E	Mo–P/Mo–E	Mo-Mo	^{31}P{^{1}H} NMR
A[7a]	2.079(2)	2.552(1), 2.463(1)	3.022(1)	−43.7
B[9,15]	2.2324(13)	2.6428(9), 2.5468(10)	3.0191(9)	30.1
C[9,15]	2.4699(14)	2.6942(9), 2.7972(9)	3.0563(11)	90.7
D[10a]	2.311(3)	2.676(2), 2.569(2)	3.039(2)	–
E[10b]	2.678(1)	2.762(1), 2.854(1)	3.114(1)	–
1	2.1447(12)	2.4249(6)	3.0347(3)	−80.11
2	2.267(8)	2.601(4), 2.572(9)	3.0530(6)	−26.63
3	2.760(2), 2.423(5)	2.519(5), 2.8088(19), 2.8132(18), 2.477(5)	3.1130(18), 3.039(2)	47.9
4	2.3808(5)	2.5740(6), 2.6340(6)	3.07173(6)	–
5	2.7504(5)	2.7455(5), 2.8513(5)	3.1107(5)	–

The molecular structures of **2** and **3** as shown in Figures 2a and 2b,c, respectively, are fully in accord with the spectroscopic assignments. The unit cell of **2** incorporated two CH_2Cl_2 molecules for each formula unit, with this composition being confirmed by elemental analysis. The Cu–P (2.2916(9)–2.434(10) Å) and Cu–As (2.526(4) Å) bond lengths are found to be similar to those observed in **1** and **4**. The observed P–As bond length of 2.647(5) Å in **2** is longer than those in {**B**$_4$}[(CuX){Cu(μ-X)}]$_2$ (X = Cl, Br) (2.240(4)–2.298(4) Å) and in the uncoordinated ligand **B** (2.2324(13) Å).[9]

On the other hand, X-ray diffraction studies show that the asymmetric unit of **3** comprises two independent molecules. The first molecule shows an η^2-coordination mode of **C** providing a tetrahedral geometry around the Cu atom (Figure 2b), whereas in the second molecule, Cu adopts a trigonal planar geometry as it binds to **C** through an η^1-coordination mode (Figure 2c). The solid-state structure indeed shows two distinct Cu–Sb bond distances of 2.760(2) (Sb1-Cu2) and 3.317(2) Å (Cu1-Sb2). Although the former is within the range of reported complexes, the latter certainly discards any kind of Cu···Sb interaction. Note that the Cu–Sb bond lenghts observed in {**C**$_4$}[(CuX){Cu(μ-X)}]$_2$ (X = Cl, Br) are between 2.667(4) and 2.771(7) Å. The P–Sb bond lengths of 2.448(5) (Sb1-P2) and 2.423(5) Å (Sb2-P6) in **3** are comparable to that of the non-coordinated complex **C** (2.469(9) Å) (Table 1).[9] To the best of our knowledge, this is the first instance to present an η^1-coordinated **C**. Further, the CSD database search shows no structural precedence of such a side-on η^2-coordination mode of **B** and **C**.

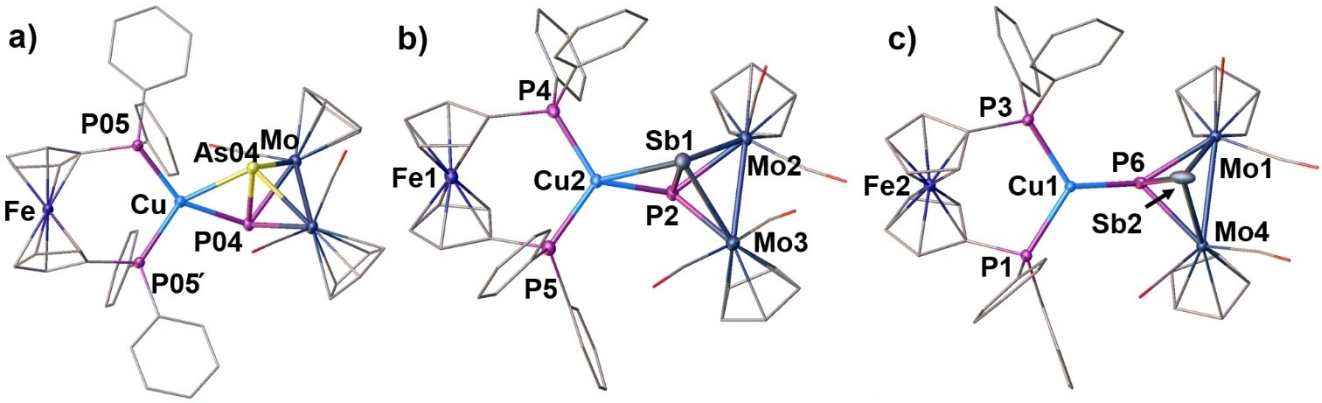

Figure 2. Solid-state structures of the cationic complexes (a) **2** and **3** in (b) and (c). Ellipsoids are drawn at 50% probability (except for C and O atoms). Anion, BF_4 and the hydrogen atoms are omitted for clarity. Selected bond lengths (Å) and angles (°) of **2**: P04-As04 2.647(5), As04-Cu 2.526(4), P04-Cu 2.434(10), P05-Cu 2.2916(9), Mo-Mo 3.0530(6), P05-Cu-P05′ 109.65(5), As04-Cu-P04 125.63(12), P05-Cu-As04 81.69(9); **3**: Sb1-P2 2.448(5), Sb2-P6 2.423(5), Mo2-Mo3 3.093(2),, Mo1-Mo4 3.1130(18), P4-Cu2 2.267(5), P3-Cu1 2.297(4), Cu(1)-P(6) 2.246(5), Cu(2)-P(2) 2.308(5), Sb1-Cu2 2.760(2), Cu1-Sb2 3.317(2), Mo2-P2 2.519(5), Mo2-Sb1 2.8088(19), Mo1-P6 2.498(5), Mo1-Sb2 2.8010(18), Sb1-Cu2-P2 123.07(12), P4-Cu2-P5 112.65(18), P6-Cu1-Sb2 90.45(19), P3-Cu1-P1 113.83(16).

Electrochemical Studies

Redox properties and subsequent one-electron oxidation chemistries of the uncoordinated **A**–**E** were reported not long since, which resulted in interesting dicationic chains or cage-like structural motifs bearing unsubstituted pnictogens.[17] This prompted us to study the cyclo-voltammograms (CVs) of **1**–**5** to compare them to the free ligand complexes to determine the coordination effect. The CVs of **1**–**5** (Figures S42-S46) reveal chemically pseudo-reversible oxidations at +0.11 V (**1**), +0.035 V (**2**), +0,24 V (**3**), +0.075 V (**4**) and +0.10 V (**5**) vs. $Cp_2Fe^{0/+}$, with the reduction peaks significantly shifted to a lower potential at −1.06 V(**1**), −1.06 V (**2**), −0.83 V (**3**), −1.19 V (**4**) and −0.74 V (**5**). The trend of a decreasing oxidation potential from **1** to **4** is in accordance with the increase in the atomic number of the element, with the only exception being **5**. Note that CVs of **A**-**E** were reported previously that showed chemically pseudo-reversible oxidations at +0.28 V (**A**), +0.19 V (**B**), +0.08 V (**C**), +0.19 V (**D**) and +0.05 V (**E**), with reduction peaks at −0.22 V (**A**), −0.31 V (**B**), −0.43 V (**C**), −0.06 V (**D**) and −0.38 V (**E**).[17] Further, the unreacted $[(dppf)Cu(MeCN)_2][BF_4]$ (Figure S47) shows two quasi-reversible oxidations (at +0.178 V and +0.91 V) and three reductions (at +0.42 V, −0.02 V and −1.4 V). As a result, the shifts in the CVs of **1**–**5** with respect to **A**-**E** can be attributed to the coordination of the tetrahedral complex (**A**-**E**) to Cu(I). A second irreversible oxidation at +0.47 V is observed for **1**, which is closer to free **A** (+0.45 V). A cyclic voltammogram, comparable to that of **1** was observed for **5**, which exhibited, however, a higher second oxidation peak at +0.96 V. Compound **2** (Figure S43) underwent a total of three oxidations (at +0.035, +0.37 and +0.88 V) and two reductions (at −1.06 and −2.1 V) which were significantly more shifted than in the case of the uncoordinated ligand complex **B** (+0.19 V, +0.45 V, +0.71 V and −0.31 V).[17b] On the other hand, the heavier analog **3** underwent a total of three oxidations (at +0.25 V, +0.62 V and +1.17 V, Figure S44) and one reduction (at −0.83 V) as opposed to the free **C**, which showed two oxidations at +0.08 V, +0.56 V and two reductions at −0.43 V, −2.16 V. Compound **4** (Figure S45) showed three oxidations (at +0.07 V, +0.26 V and +0.79 V) and three reductions (at −0.012 V, −0.31 V and −1.2 V) altogether.[18]

Quantum Chemical Calculations

To gain some insight into the bonding of compounds **1**–**5**, quantum chemical calculations were performed including the solution effect (CH_2Cl_2) on the grounds of DFT methods using ωB97X–D/def2-SVP level of theory (see computational details in the supporting information and Table 2). The optimized geometries of **1**, **2**, **4** and **5** corroborated satisfactorily with the X-ray geometries. However, the solution phase ground state optimized geometry of **3** exhibits only an η^2-coordination mode of **C**. This may be attributed to the packing effect that may exist in the solid-state structure of **3** (Table 3). Note, that a high HOMO-LUMO gap of ca. 6.7 eV has been computed for all the compounds. The natural bond orbital (NBO) analyses of **1**–**5**, demonstrate that the Cu(I) ion binds to the σ(P–E/E–E) orbital of the tetrahedral-Mo_2PE/Mo_2E_2 units (e.g. LMO 251 of **1** is shown in figure 3d). Further, the NBO analysis revealed addi-

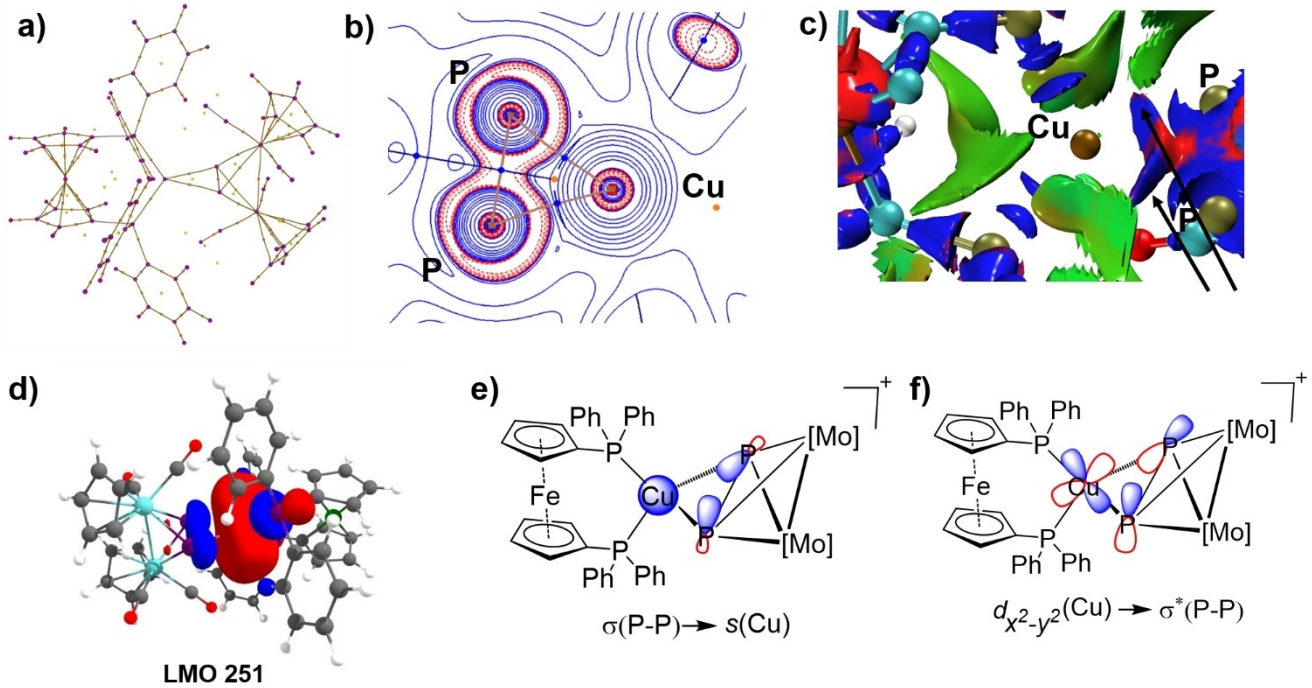

Figure 3. Probing the bonding in **1**. (a) Molecular graph. (b) Topology of the Laplacian of the electron density in the {Cu-P_2} plane. Positive values depicted in red dashed curves and negative values in solid blue curves. (c) Interaction Region Indicator (IRI) plot (isosurface at 0.98 au.). (d) Selected localized molecular orbital (LMO) representing the Cu···P_2 interaction. (e) and (f) Showing the donor acceptor interactions (isosurfaces at 0.03 au) as obtained from the NBO analysis.

Table 2. Calculated charges and AIM (atoms in molecules) properties of selected atoms and bonds of **A**-**E** and **1**–**5**.

parameters	A	B	C	D	E	1	2	3	4	5
q_{Mo}	−0.52 −0.50	−0.53 −0.54	−0.47 −0.56	−0.56 −0.56	−0.62 −0.62	−0.50 −0.50	−0.52 −0.53	−0.48 −0.56	−0.55 −0.55	−0.62 −0.62
q_P[a]	0.14 0.15	0.08	−0.15	–	–	0.05 0.05	−0.02	−0.23	–	–
q_E[b]	–	0.30	0.7	0.23, 0.23	0.39	–	0.21	0.64	0.14, 0.14	0.34, 0.34
q_{Cu}	–	–	–	–	–	0.753	0.749	0.731	0.744	0.703
Pop (Mo_{val})	6.44	6.45 6.46	6.39 6.49	6.48, 6.48	6.54, 6.54	6.42, 6.42	6.44, 6.45	6.40, 6.48	6.65	6.54, 6.54
Pop (P_{val})[a]	4.82	4.89	5.12	–	–	4.91, 4.91	4.98	5.18	–	–
Pop (E_{val})[b]	–	4.67	4.27	4.74, 4.74	4.59, 4.59	–	4.75	4.34	4.83, 4.83	4.63, 4.63
Pop (Cu_{val})[b]	–	–	–	–	–	10.22	10.22	10.24	10.23	10.27
P–P/P–E/E-E[c]	2.09	2.21	2.39	2.31	2.68	2.16	2.28	2.46	2.38	2.76
P–Cu/ E-Cu[c]	–	–	–	–	–	2.43 2.44	2.41, 2.55	2.30, 2.89	2.52, 2.52	2.69, 2.69
WBI (P–P/P–E/E–E)	1.19	1.16	1.17	1.15	1.11	1.08	1.04	1.04	1.02	0.96
WBI (P–Cu/E–Cu)	–	–	–	–	–	0.16, 0.16	0.18, 0.16	0.22, 0.11	0.17, 0.17	0.20, 0.20
$E^{(2)}$ (P–P/P–E/E–E)→Cu[d]					–	22.8	27.9	30.4	32.0	58.8
$E^{(2)}$ Cu→(P–E/E–E)[d]	–	–	–	–	–	6.9	7.8	5.2	7.8	6.5
ρ(r) (P–P/P–E/E–E)	0.132	0.112	0.088	0.099	0.067	0.116	0.097	0.078	0.086	0.058
ρ(r) (Cu–P/E)	–	–	–	–	–	0.055 0.055	0.057 0.049	0.067[e]	0.051 0.051	0.046 0.046
∇^2(r) (P–P/P–E/E–E)	−0.194	−0.067	0.035	−0.040	0.003	−0.119	−0.024	0.047	−0.008	0.017
∇^2(r) (Cu–P/E)	–	–	–	–	–	0.119 0.120	0.123 0.086	0.160[e]	0.087 0.087	0.043 0.043
H(r) (P–P/P–E/E–E)	−0.089	−0.062	−0.037	−0.049	−0.258	−0.068	−0.046	−0.029	−0.038	−0.019
H(r) (Cu–P/E)	–	–	–	–	–	−0.011 −0.011	−0.011 −0.012	−0.014[E]	−0.012 −0.012	−0.013 −0.013
ELF (P–P/P–E/E–E)	0.853	0.730	0.545	0.703	0.595	0.805	0.675	0.499	0.645	0.525
ELF(Cu–P/E)	–	–	–	–	–	0.236, 0.236	0.251 0.254	0.254[e]	0.264 0.264	0.326 0.326
$E_{H\text{-}L}$	7.15	7.05	6.68	6.99	6.66	6.92	6.90	6.69	6.93	6.74

[a] qp for qp-p or qp-E. [b] qE for qp-E or E–E bonds. [c] optimized bond lengths in Å. [d] Second-order-perturbation-energy (in kcal/mol) obtained from the NBO analysis. Electron density ρ(r) [e Å^{-3}], Laplacian of electron density $\nabla^2\rho$(r) [e Å^{-5}], total energy density H(r) electron localization function (ELF). [e] BCP along the Cu–Sb bond was not observed.

tional factors contributing to the stability of compounds **1**–**5**. The results of the second-order perturbation theory analysis reveal highly stabilizing interactions between the bonding P–E/E–E NBOs and the empty Cu-orbitals rather than back-donation into the σ* (P–E/E–E)-orbital (for example 22.8 versus 6.9 kcal/mol for **1**, Table 2, the simplified pictures are shown in Figures 3e and 3f). The calculated Wiberg bond index (WBI) values of the P–E/E–E bonds in **1**–**5** are consistent with the single bonds, however, are found slightly lesser than the corresponding WBI values calculated for the uncoordinated complexes **A**–**E**. For example, the WBI value of 1.19 for the P–P bond in uncoordinated complex, **A** is reduced to 1.08 in complex **1**. This is consistent with the depletion of the electron density of the P–E/E–E bonds while coordinating with the Cu(I) center. On the other hand, lower WBI values (ca. 0.11–0.22) have been computed for the P–Cu/E–Cu bonds. The NBO charge analysis shows that while going from **A** to **E**, negative charges are accumulated on the P and Mo centres while positive charges are developed on E (As, Sb) due to the increasing metallic character of E. Additionally, the topology of the total electron density in **1**–**5** has been assessed by the atoms-in-molecules (AIM) approach. The electron density (ρ(r)) is slightly decreased along the P–E/E–E bonds in **1**–**5**, compared to the free ligands **A**–**E**. Note that the ELF values (electron localization function), at the bond-critical points (BCP, (3,–1), blue), of the P/E–Cu bonds are calculated to be in the range of 0.2–0.3, whereas those of the P–E/E–E bonds are in the higher range of 0.49–0.8 (in a scale between 0 and 1). However, the negative values of the energy density (H(r)) suggested a covalent character for the P/E–Cu interactions. Analysis of the

Table 3. Crystallographic data for compounds **1**–**5**.

	1	2	3	4	5
Formula	$C_{50}H_{42}BCl_4CuF_4FeMo_2O_4P_4$	$C_{50}H_{42}AsBCl_4CuF_4FeMo_2O_4P_3$	$C_{96}H_{76}B_2Cu_2F_8Fe_2Mo_4O_8P_6Sb_2$	$C_{50}H_{42}As_2BCl_4CuF_4FeMo_2O_4P_2$	$C_{50}H_{42}BCl_4CuF_4FeMo_2O_4P_2Sb_2$
$D_{calc.}$/g cm^{-3}	1.770	1.816	1.870	1.873	1.921
m/mm^{-1}	10.185	10.538	2.043	2.751	2.414
Formula Weight	1370.59	1414.54	2583.04	1458.49	1552.15
Colour	clear orange	clear yellow	clear orange	clear orange	clear orange
Shape	block-shaped	plate-shaped	plate-shaped	block-shaped	block-shaped
Size/mm^3	0.31×0.24×0.23	0.15×0.07×0.05	0.53×0.33×0.04	0.12×0.10×0.08	0.26×0.13×0.07
T/K	123.00(10)	123.01(10)	100.00(10)	100.01(10)	100.00(10)
Crystal System	monoclinic	monoclinic	monoclinic	monoclinic	orthorhombic
Space Group	*C*2/*c*	*C*2/*c*	*Pn*	*C*2/*c*	*Pna*2$_1$
a/Å	12.29940(10)	12.3535(2)	11.7572(2)	12.35490(10)	16.92620(10)
b/Å	29.4704(3)	29.5203(3)	28.3550(4)	29.5777(3)	19.09000(10)
c/Å	14.4344(2)	14.4393(2)	13.7630(2)	14.4070(2)	16.60670(10)
a/°	90	90	90	90	90
b/°	100.6450(10)	100.6620(10)	90.419(2)	100.6900(10)	90
g/°	90	90	90	90	90
V/Å^3	5141.97(10)	5174.80(12)	4588.12(12)	5173.37(10)	5365.98(5)
Z	4	4	2	4	4
Z'	0.5	0.5	1	0.5	1
Wavelength/Å	1.54184	1.54184	0.71073	0.71073	0.71073
Radiation type	Cu K_α	Cu K_α	Mo K_α	Mo K_α	Mo K_α
Q_{min}/°	3.953	2.994	2.270	2.112	2.022
Q_{max}/°	66.782	75.310	37.813	39.327	44.835
Measured Refl.	22880	20844	66530	35498	208544
Independent Refl.	4521	5247	37366	12627	42710
Reflections with I > 2(I)	4507	4722	35942	11001	38259
R_{int}	0.0416	0.0319	0.0285	0.0172	0.0269
Parameters	350	358	1172	349	641
Restraints	50	62	170	0	2
Largest Peak	0.501	0.922	2.319	0.650	1.629
Deepest Hole	−0.593	−1.474	−3.257	−0.468	−1.099
GooF	1.079	1.169	1.085	1.050	1.053
wR_2 (all data)	0.0730	0.1224	0.2275	0.0481	0.0495
wR_2	0.0729	0.1209	0.2262	0.046	0.0483
R_1 (all data)	0.0267	0.0433	0.0872	0.0271	0.0316
R_1	0.0266	0.0403	0.0852	0.0205	0.0254

ELF computed for the total electrons of **1** revealed disynaptic valence basins for Cu–P and P–P (Figure S6, Table S2). Figure 3b shows the Laplacian of the electronic charge distribution $\nabla^2\rho(r)$ in the {Cu-P_2} plane of compound **1**. Whereas charge accumulation ($\nabla^2\rho(r) < 0$, red dashed lines) area along the P–P bond has been found, spherical areas of relative charge depletion ($\nabla^2\rho(r) > 0$, blue solid lines) around the Cu center could be observed. Note that deformation of the charge density of the P–P bond by the Cu(I) have been observed, indicating Cu···P_2 bonding. Nonetheless, the molecular graph (Figure 3a, molecular graph of **1**), in general, describes the overall bonding situation satisfactorily, showing two BCPs along the P–Cu bonds and an RCP (ring-critical point, (3, +1), orange) within the {P_2Cu} triangle. The interaction between the Cu center and the ligands **A**–**E** in compounds **1**–**5** is also supported by the visual analysis of the interaction region indicator diagram (IRI, Figure 3c) that identified the regions of overlapping electron densities.

Conclusions

In summary, syntheses and characterizations of a series of isomorphous compounds with the general molecular formula [(dppf)Cu(μ_3,$\eta^{2:2:2}$-E_2{CpMo(CO)$_2$}$_2$][BF_4] (E = P, As, Sb) and [(dppf)Cu(μ_3,$\eta^{2:2:2}$-PE{CpMo(CO)$_2$}$_2$][BF_4] (E = As, Sb) are reported where the tetrahedral dimolybdenum complexes utilized a rare side-on η^2-coordination mode. In addition, an unusual η^1-coordination mode is observed for the first time in the solid-state structure of [(dppf)Cu(μ_3,$\eta^{2:2:1}$-PSb{CpMo(CO)$_2$}$_2$][BF_4] revealing a unique lone pair coordination of one P atom. Theoretical calculations provide substantial insight into the structure and bonding of the reported complexes. Ongoing investigations including the heavier Bi analogs and a more flexible coordination sphere of Ag are in progress.

Acknowledgements

This work was supported by the Deutsche Forschungsgemeinschaft within the project Sche 384/42-1. BM thanks the Alexander von Humboldt Foundation for his postdoctoral fellowship. Robert Szlosek is gratefully acknowledged for his generous help with the CV measurements. We thank Christoph Riesinger for the final X-ray structural refinement and Dr. Gábor Balázs for useful discussions. Open Access funding enabled and organized by Projekt DEAL.

Conflict of Interests

The authors declare no conflict of interest.

Data Availability Statement

The data that support the findings of this study are available in the supplementary material of this article.

Keywords: antimony · arsenic · coordination-compounds · chelating complexes · copper · phosphorus

[1] a) O. J. Scherer, *Acc. Chem. Res.* **1999**, *32*, 751–762; b) M. Scheer, *Dalton Trans.* **2008**, 4372–4386.
[2] a) R. W. Saalfrank, B. Demleitner, in *Transition Metals in Supramolecular Chemistry; Perspectives in Supramolecular Chemistry*, Vol. 5, (Ed. J.-P. Sauvage), John Wiley & Sons Ltd., Chichester, England, **1999**; pp 1–51; b) M. Fujita, M. Tominaga, A. Aoai, B. Therrien, *Acc. Chem. Res.* **2005**, *38*, 369–378; c) T. R. Cook, Y.-R. Zheng, P. J. Stang, *Chem. Rev.* **2013**, *113*, 734–777.
[3] a) E. Peresypkina, A. Virovets, M. Scheer, *Coord. Chem. Rev.* **2021**, *446*, 213995; b) A. V. Virovets, E. Peresypkina, M. Scheer, *Chem. Rev.* **2021**, *121*, 14485–14554.
[4] a) J. Bai, A. V. Virovets, M. Scheer, *Angew. Chem. Int. Ed.* **2002**, *41*, 1737–1740; *Angew. Chem.* **2002**, *114*, 1808–1811; b) J. Bai, E. Leiner, M. Scheer, *Angew. Chem. Int. Ed.* **2002**, *41*, 783–786; *Angew. Chem.* **2002**, *114*, 820–823; c) L. J. Gregoriades, B. K. Wegley, M. Sierka, E. Brunner, C. Gröger, E. V. Peresypkina, A. V. Virovets, M. Zabel, M. Scheer, *Chem. Asian J.* **2009**, *4*, 1578–1587; d) E.-M. Rummel, M. Eckhardt, M. Bodensteiner, E. V. Peresypkina, W. Kremer, C. Groger, M. Scheer, *Eur. J. Inorg. Chem.* **2014**, 1625–1637; e) C. Heindl, A. Kuntz, E. V. Peresypkina, A. V. Virovets, M. Zabel, D. Ludeker, G. Brunklaus, M. Scheer, *Dalton Trans.* **2015**, *44*, 6502–6509; f) M. Fleischmann, S. Welsch, E. V. Peresypkina, A. V. Virovets, M. Scheer, *Chem. Eur. J.* **2015**, *21*, 14332–14336; g) C. Heindl, E. V. Peresypkina, D. Ludeker, G. Brunklaus, A. V. Virovets, M. Scheer, *Chem. Eur. J.* **2016**, *22*, 2599–2604; h) M. E. Moussa, S. Welsch, M. Lochner, E. Peresypkina, A. V. Virovets, M. Scheer, *Eur. J. Inorg. Chem.* **2018**, 2689–2694.
[5] a) J. Bai, A. V. Virovets, M. Scheer, *Science* **2003**, *300*, 781–783; b) M. Scheer, A. Schindler, R. Merkle, B. P. Johnson, M. Linseis, R. Winter, C. E. Anson, A. V. Virovets, *J. Am. Chem. Soc.* **2007**, *129*, 13386–13387; c) S. Welsch, C. Groger, M. Sierka, M. Scheer, *Angew. Chem. Int. Ed.* **2011**, *50*, 1435–1438; *Angew. Chem.* **2011**, *123*, 1471–1474; d) F. Dielmann, C. Heindl, F. Hastreiter, E. V. Peresypkina, A. V. Virovets, R. M. Gschwind, M. Scheer, *Angew. Chem. Int. Ed.* **2014**, *53*, 13605–13608; *Angew. Chem.* **2014**, *126*, 13823–13827; e) C. Heindl, E. V. Peresypkina, A. V. Virovets, W. Kremer, M. Scheer, *J. Am. Chem. Soc.* **2015**, *137*, 10938–10941; f) F. Dielmann, E. V. Peresypkina, B. Krämer, F. Hastreiter, B. P. Johnson, M. Zabel, C. Heindl, M. Scheer, *Angew. Chem. Int. Ed.* **2016**, *55*, 14833–14837; *Angew. Chem.* **2016**, *128*, 15053–15058; g) C. Heindl, E. Peresypkina, A. V. Virovets, I. S. Bushmarinov, M. G. Medvedev, B. Krämer, B. Dittrich, M. Scheer, *Angew. Chem. Int. Ed.* **2017**, *56*, 13237–13243; *Angew. Chem.* **2017**, *129*, 13420–13426.
[6] a) M. Scheer, J. Bai, B. P. Johnson, R. Merkle, A. V. Virovets, C. E. Anson, *Eur. J. Inorg. Chem.* **2005**, 4023–4026; b) M. Scheer, A. Schindler, J. Bai, P. Johnson, R. Merkle, R. Winter, A. V. Virovets, E. V. Peresypkina, V. A. Blatov, M. Sierka, H. Eckert, *Chem. Eur. J.* **2010**, *16*, 2092–2107; c) M. E. Moussa, M. Piesch, M. Fleischmann, A. Schreiner, M. Seidl, M. Scheer, *Dalton Trans.* **2018**, *47*, 16031–16035.
[7] a) O. J. Scherer, H. Sitzmann, G. Wolmershäuser, *J. Organomet. Chem.* **1984**, *268*, C9–C12; b) O. J. Scherer, J. Schwalb, H. Sitzmann, *Inorg. Synth.* **1990**, *27*, 224–227.
[8] a) M. Scheer, L. J. Gregoriades, M. Zabel, J. Bai, I. Krossing, G. Brunklaus, H. Eckert, *Chem. Eur. J.* **2007**, *28*, 282–295; b) M. Scheer, L. Gregoriades, J. Bai, M. Sierka, G. Brunklaus, H. Eckert, *Chem. Eur. J.* **2005**, *11*, 2163–2169.
[9] J. E. Davies, L. C. Kerr, M. J. Mays, P. R. Raithby, P. K. Tompkin, A. D. Woods, *Angew. Chem. Int. Ed.* **1998**, *37*, 1428–1429; *Angew. Chem.* **1998**, *110*, 1473–1475.
[10] a) P. J. Sullivan, A. L. Rheingold, *Organometallics* **1982**, *1*, 1547–15490; b) J. R. Harper, A. L. Rheingold, *J. Organomet. Chem.* **1990**, *390*, C36–C38.
[11] a) P. K. Mehrotra, R. Hoffmann, *Inorg. Chem.* **1978**, *17*, 2187–2189; b) P. Pyykko, *Chem. Rev.* **1997**, *97*, 597–636; c) K. M. Merz, R. Hoffmann, *Inorg. Chem.* **1988**, *27*, 2120–2127; d) H. Schmidbaur, A. Schier, *Angew. Chem. Int. Ed.* **2015**, *54*, 746–784; *Angew. Chem.* **2015**, *127*, 756–797.
[12] a) H. V. Ly, M. Parvez, R. Roesler, *Inorg. Chem.* **2006**, *45*, 345–351; b) M. E. Moussa, M. Seidl, G. Balázs, M. Hautmann, M. Scheer, *Angew. Chem. Int. Ed.* **2019**, *58*, 12903–12907; *Angew. Chem.* **2019**, *131*, 13035–13039; c) M. E. Moussa, J. Schiller, E. Peresypkina, M. Seidl, G. Balázs, P. Shelyganov, M. Scheer, *Chem. Eur. J.* **2020**, *26*, 14315–14319; d) J. Schiller, A. Schreiner, M. Seidl, G. Balázs, M. Scheer, *Chem. Eur. J.* **2020**, *26*, 14570–14574; e) P. A. Shelyganov, M. E. Moussa, M. Seidl, M. Scheer, *Angew. Chem. Int. Ed.* **2023**, *62*, e202215650; *Angew. Chem.* **2023**, *135*, e202215650.
[13] a) G. Bandoli, A. Dolmella, *Coord. Chem. Rev.* **2000**, *209*, 161–196; b) D. J. Young, S. W. Chien, T. S. A. Hor, *Dalton Trans.* **2012**, *41*, 12655–12665; c) M. Mohankumar, M. Holler, J.-F. Nierengarten, J.-P. Sauvage, *Chem. Eur. J.* **2012**, *18*, 12192–12195; d) U. Albold, C. Hoyer, N. I. Neuman, S. Sobottka, A. S. Hazari, G. K. Lahiri, B. Sarkar, *Inorg. Chem.* **2019**, *58*, 3754–3763.
[14] N. Elgrishi, K. J. Rountree, B. D. McCarthy, E. S. Rountree, T. T. Eisenhart, J. L. Dempsey, *J. Chem. Educ.* **2018**, *95*, 197–206.
[15] L. Dütsch, C. Riesinger, G. Balázs, M. Scheer, *Chem. Eur. J.* **2021**, *27*, 8804–8810.
[16] C. R. Groom, I. J. Bruno, M. P. Lightfoot, S. C. Ward, *Acta Crystallogr. Sect. B* **2016**, *72*, 171–179.
[17] a) L. Dütsch, M. Fleischmann, S. Welsch, G. Balázs, W. Kremer, M. Scheer, *Angew. Chem. Int. Ed.* **2018**, *57*, 3256–3261; *Angew. Chem.* **2018**, *130*, 3311–3317; b) L. Dütsch, C. Riesinger, G. Balázs, M. Seidl, M. Scheer, *Chem. Sci.* **2021**, *12*, 14531–14539.
[18] Note that the cyclic voltammograms of **2**–**4** were badly resolved which may be due to the complex reactions that took place *in-situ*.

Manuscript received: October 20, 2023
Accepted manuscript online: December 27, 2023
Version of record online: ■■, ■■

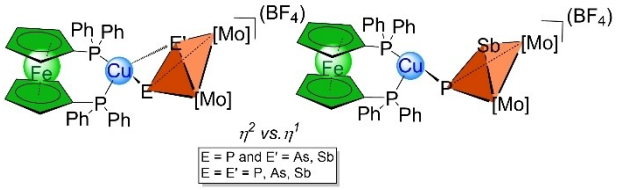

The coordination chemistry of the homo- and hetero-dinuclear tetrahedral molybdenum complexes $[Mo_2E_2]$ (E = P, As, Sb) and $[Mo_2PE]$ (E = As, Sb) towards $[(dppf)Cu(MeCN)_2][BF_4]$ are presented showing structural evidence of the side-on η^2-coordination of the tetrahedral $[Mo_2PE]$ and $[Mo_2E_2]$ complexes and a rare η^1-coordination of the $[Mo_2PSb]$ complex.

*Dr. B. Mondal, Prof. Dr. M. Scheer**

1 – 9

Cu(I) Complexes Comprising tetrahedral Mo_2E_2 or Mo_2PE units (E = P, As, Sb) as Chelating Ligands